Shear strength of rock, rock joints and rock masses – problems and some solutions

N.R.Barton
Nick Barton & Associates, Oslo, Norway

ABSTRACT: These three important topics, each deserving separate volumes, even when summarized, can only be treated in a single article by linking them. The all-encompassing shear strength of rock masses cannot be described with advanced algebra as in Hoek-Brown, nor as linear Mohr-Coulomb, each of which are *a priori* estimates rather than the desirable *a posteriori* based on experience. The highly non-linear shear strength of intact rock, which has finally been defined as strongly deviated from Mohr-Coulomb, and with more curvature than Hoek-Brown, is the component which fails at small strain. Deep in the crust rocks may be ductile or at their critical state. The very different and weaker joints or fractures provide stability problems in civil and mining engineering, and help maintain some permeability in fractured reservoirs. Joints are highly anisotropic features. They exhibit large differences between their high normal stiffness, and their low, scale-dependent shear stiffness. Joints obviously reach their peak shear strength at larger shear strain than intact rock, and their frictional strength 'remains' after cohesion is lost, as in the words of Müller 1966. It is not correct to add the cohesive strength of the intact rock and the shear resistance of the joints, as in c plus sigma-n tan-phi, nor as in the non-linear form of Hoek-Brown. A third shear strength component may kick-in at larger shear strain: the lower frictional strength of clay-filled discontinuities, such as in the neighbourhood of faults. Finally there is the wide-reaching problem of stress transformation, from principal stresses to normal and shear stress components on a plane. Dilation, shearing and the very presence of the plane violates the theoretical assumptions.

1 INTRODUCTION

1.1 *The importance of rock and rock joints*

Why is shear strength, consisting of *cohesion, friction, and dilation* ultra-important to earth-dwellers? Basically because without their variety there would be no mountains, no river valleys, no deserts, and no oil or gas. Since we are blessed with the variability of these three parameters, we have variable scenery ranging from mountains, to rolling hills, to deserts, and mountain- and sea-cliffs as the source of screes, beaches and eventual inland or coastal sand-dunes. The cycle continues with post-lithification (and post-tectonic) fracturing, breakage of cohesion, block formation, and once more: mobilized friction and dilation. The three strength components do not occur simultaneously, so cohesive and frictional strength need to be partially separated, by degrading cohesion, mobilizing friction, then mobilizing dilation.

1.2 *Economic influence of shear strength*

It is interesting to consider that petroleum reserves have been retained (for our present benefit, and possible downfall), due to cap-rock intolerance of shear stress. Shales and salt therefore exhibit higher levels of minimum principal stress compared to the lower σ_{min} of stiffer petroleum bearing sediments. Furthermore, petroleum reserves have also been retained due to clay-sealing along fault zones, thanks to the weakest product of weathering or hydrothermal alteration. At shallow depth the above minimum stress anisotropy is reversed, and the stiffer beds will tend to attract higher minimum stress than cap-rock shale or salt (Barton, 2006).

1.3 *Economic influence of joint behaviour*

Rock joints or natural fractures provide conductivity during water and petroleum production, by connecting the fluid-storing matrix to the wells. When fracing *oil-shales* for shale-gas production, the incipient (or very tightly closed) jointing may apparently shear and dilate enough to unlock the vast potential reserves in an otherwise impermeable looking rock mass. Micro-seismic activity in *geothermal* reservoirs, also suggests that jointing is mobilized, sometimes in unexpected ways when today's joint orientation is no longer consistent with today's rotated

major stress axes. The cold injected water then may bypass the intended production well, due to 'capture' by the unexpectedly oriented joint set.

1.4 Non-linear components of rock mass strength

Figure 1 illustrates a collection of non-linear, shear strength envelopes, which for convenience have been collected in one diagram, with an *empirically linking* equation of shear strength in the form:

$$\tau = \sigma_n \tan [X.\log_{10} Y + Z] \qquad (1)$$

By their very nature these typical components of a rock mass will usually be loaded at a wide variety of confining stress, or normal stress levels, due to their variable stiffness and strength. Intact 'bridges' will attract higher stress, due to their higher resistance. The 'Jr/Ja' filled discontinuities will tolerate least load, so could fail a slope 'easily' if they dominate.

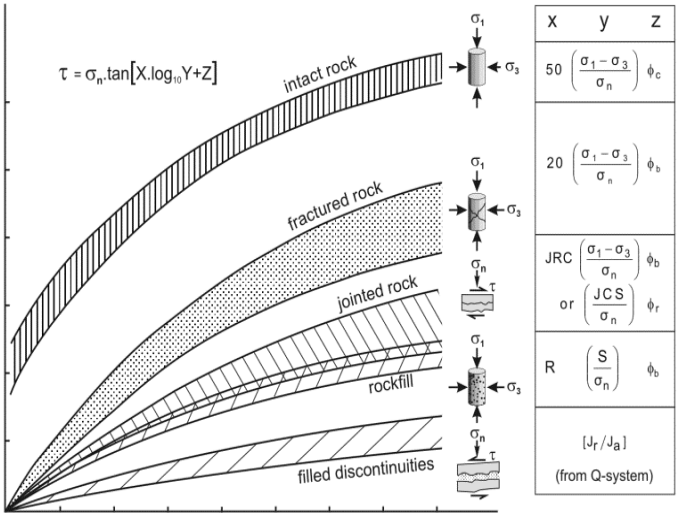

Figure 1 The five shear strength envelopes represent the potential components of shear strength *for a rock mass.* From top down, and at increasing magnitudes of strain, each component will supply shear resistance in turn, with each falling towards a residual strength with eventual increased deformation. The shear strength of rock masses is a composite affair. It is not so 'simple' as H-B/GSI algebra. (From Barton, 1973, 1976, 2006)

2 SHEAR STRENGTH OF INTACT ROCK

2.1 *Low tolerance of shear stress*

In the introduction, the economic importance of salt and shale as cap-rocks was emphasized. It is appropriate to start by showing their low position on the 'tolerance of shear stress' scale, as illustrated in Figure 2. The relative weakness of shale is especially important, ever since *fracing* from horizontal holes has given remarkably stimulated production, for probable deformation-based reasons discussed later. The linear representation of strength by Swolfs, 1977 (Figure 2) is clearly an over-simplification of

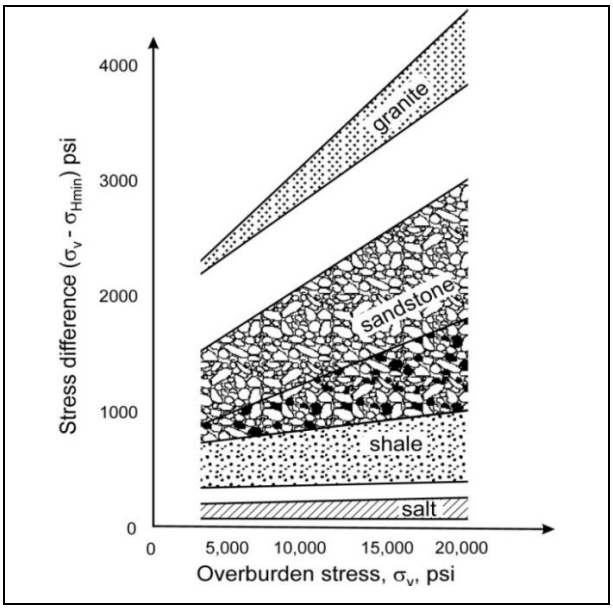

Figure 2 Relative shear strength trends for salt, shale, sandstone and granite. Linear approximations, after Swolfs, 1977.

reality when the over-burden range of stress of approx. 35-140 MPa (≈ 1.5-5.5 km depth) is considered. The strength envelopes will be strongly curved.

2.2 *Critical state concept for high stress*

When performing a wide-reaching review of the shear strength of both intact and jointed rock in the mid-seventies, the writer was struck by the strong non-linearity of the 'complete' shear strength envelopes. All the high pressure testing of Byerlee and Mogi seemed to confirm this. The examples given in Figure 3, from Mogi, 1966, are for various (dry) *carbonate* rocks. Of course they also extend beyond stress levels of interest in petroleum reservoirs.

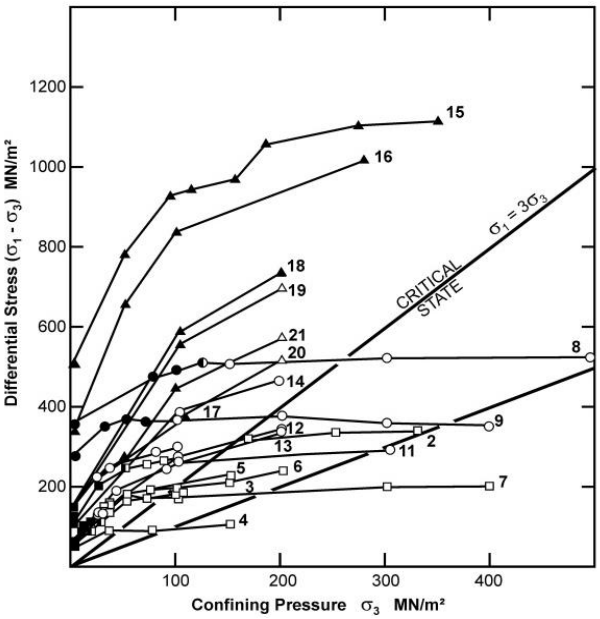

Figure 3 Strong non-linearity is also seen in petroleum reservoir depth range. Carbonate rocks tested by Mogi, 1966. Note the gradient of the critical state line, suggested in Barton, 1976.

These high-pressure triaxial tests on dry carbonate rocks, and numerous other data from Byerlee, 1968, gave the writer the idea of a 'critical state' approach to shear strength limits. The critical state line has a gradient of $\tan^{-1}(½)$, or 26°.The explanation of this term is clarified graphically in Figure 4.

The horizontal part of the shear strength envelopes for these and other rocks, suggested the following simple relation:

$$\sigma_{1\,max} = 3\,\sigma_{3\,critical} \qquad (2)$$

It will be noted that the uniaxial (unconfined) circle (#2) and the critical confining pressure circle (#4) are drawn as nearly tangent to one another. This potential simplicity has recently been confirmed by Singh et al., 2011, who found that the majority of rocks exhibited this tendency. (See also Figure 6).

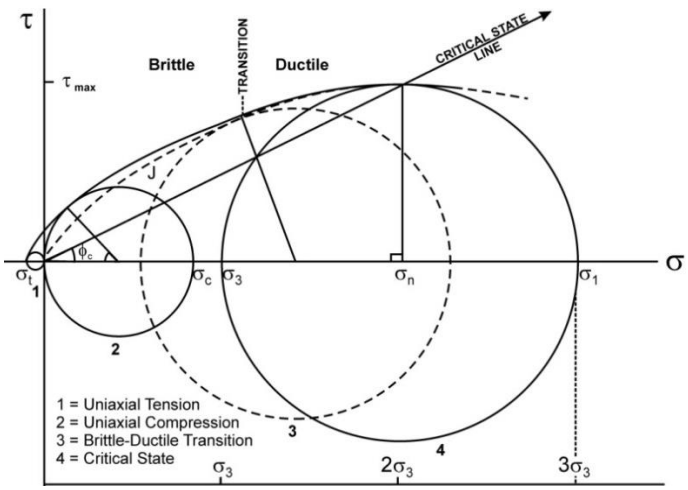

Figure 4 The illustrated 'critical state line' concept was suggested by Barton (1976) as a result of the strong non-linearity exhibited by data sets such as those reproduced in Figure 3.

This critical state based simplicity has recently been used by Singh et al. (2011) to derive the equations giving the *correct deviation* from linear Mohr-Coulomb. The new 'Singh-Singh' criterion demonstrates that just a few triaxial tests at low confining pressure give the complete strength envelope, also showing greater curvature than Hoek-Brown (see Figure 5 example). For Hoek-Brown, triaxial tests over a wider range of confining pressure are needed.

2.3 *Non-linearity more realistic than M-C*

Tight oil-shales and naturally fractured reservoirs in carbonate rocks usually produce from several kilometers depth, with or without stimulation by fracing or water-drive. Due to necessary matrix porosity, the matrix is generally weaker than is typical for basement rocks. The potential pore pressure reduction of 10's of MPa during the life of a petroleum reservoir may mean an effective stress increase which is a significant proportion of the strength of the matrix. The *inevitable non-linear intact rock shear strength behaviour* should not then be ignored.

It is quite clearly unrealistic to continually utilize a linear Mohr-Coulomb strength criterion, as seen so often in petroleum service company literature. It makes for simplicity but does not reflect reality.

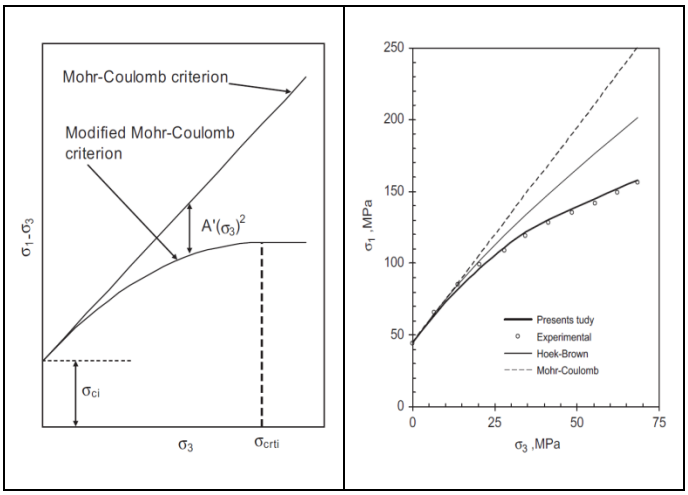

Figure 5 The objective of the Singh et al., 2011 non-linear criterion of shear strength is shown on the left, and an example is shown on the right. Tests at low confining pressure suffice.

2.4 *Conjugate joint angles vary with depth or stress*

It is now common practice for structural geologists working for oil companies to utilize *drone-photography* when recording the jointing/fracturing on pavements above naturally fractured reservoirs. These pavements may be analogues for the assumed joint or fracture networks at reservoir depths of several kilometers. (Joints/fractures used equivalently).

These fracture pavement studies are therefore important sources of information for fracture network construction, seeing the dominance of certain sets. Remarkably, no differentiation of mechanical properties seems to be applied so far, just geometrical structural relationships, potential connectivity etc.

Due to the much higher stress at reservoir depths, and due to the range of effective stresses to which the reservoir rocks may be subjected during the life of a field, the non-linearity of strength envelopes and the changing conjugate joint angles with stress or depth need to be considered. With linear Mohr-Coulomb this is not a very enlightening exercise.

The very small circles in Figure 6 represent the peak strength of fractures, and the dotted curved envelope, drawn into the inadmissible area for reasons of clarity, was used to demonstrate the maximum *empirical* strength of (rough) rock fractures (Figure 1).

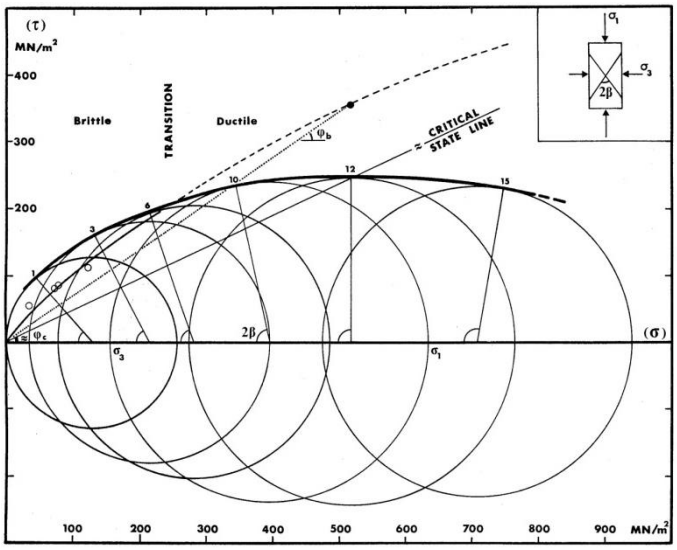

Figure 6 A complete set of Mohr circles for high-pressure tests on strong (UCS = 250 MPa) limestones derived from Byerlee, 1968 data reproduced by Barton, 1976. Note addition of critical state line. Note also the progression of the conjugate-fracture angle 2β towards 90° with increasing depth or confinement.

The strong non-linearity of shear strength envelopes should not be ignored when producing from a reservoir in weaker, more porous carbonates (or shales) with a possible life-time 20-40 MPa change of effective stress. The friction angle cannot be constant!

2.5 *A linear equation for non-linear behaviour*

A conveniently simple *linear* equation, which describes the *non-linear* shear strength behaviour of intact rock over a range of confining pressure from zero (uniaxial), through the brittle-ductile transition, and up to the critical (maximum strength) state was derived by Barton 1976, and appears to have been over-looked up to now. It had the following simplest possible form:

$$(\sigma_1 - \sigma_3)/\sigma_c = M\,\sigma_3/\sigma_1 + 1.0 \qquad (3)$$

The respective gradients M (shown in Figure 7), for Solenhofen limestone Oak Hall limestone, Nahant gabbro and Westerly granite, as tested and reported by Byerlee 1968, showed a logical progression of 3, 7, 9 and 30 as strength increased.

Figure 8 shows brittle and ductile behaviour symbols, and a suggested Byerlee, 1968 curved transition between the two states. The diagonal line at 45° is the proposed Barton, 1976 *critical state line*, which is the vertical 'limit' in Figure 7: $\sigma_{3\,crit}/\sigma_{1\,max} = 0.333$. The above critical state concept, and the key development of Singh et al., 2011 in defining *deviation from Mohr-Coulomb*, suggests good alternatives to the well-known criteria of Figure 9.

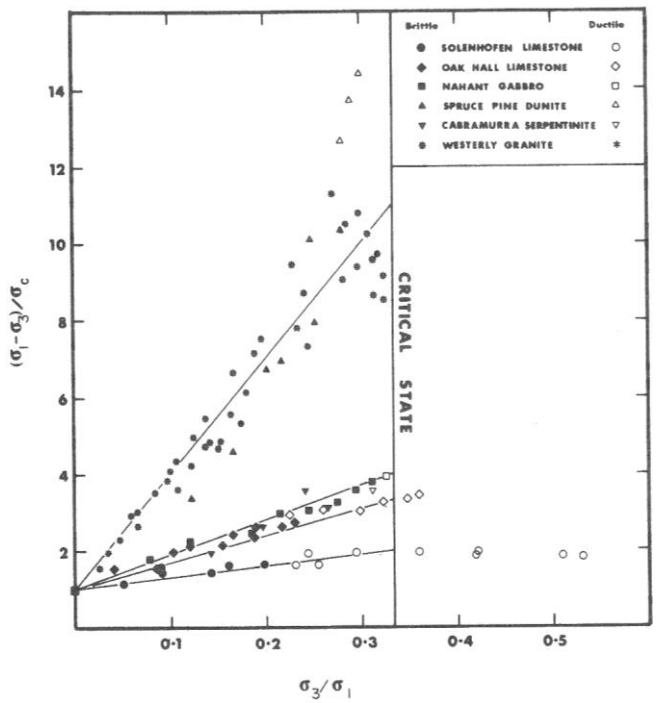

Figure 7 A method of expressing the non-linear shear strength envelopes shown in Figure 8 in a linear form, with logical differentiation of gradients between the stronger and weaker rock types. Note brittle and ductile differentiation, from the high pressure triaxial data of Byerlee, 1968.

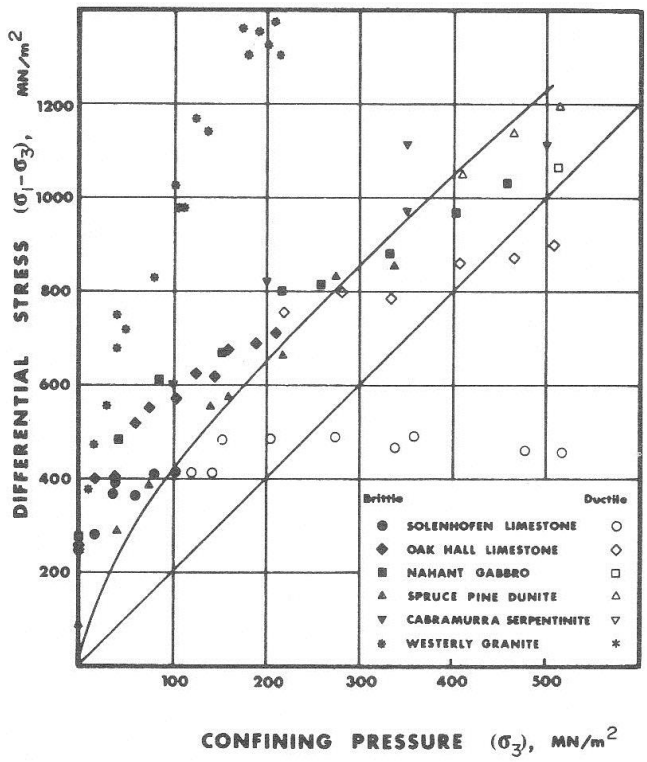

Figure 8 This conventionally plotted differential stress versus confining pressure data for six rock types is the source of the linear envelopes shown in Figure 7.

It is important to finish this treatment of the shear strength of *intact rock* by pointing out that this potential component of the shear strength of *rock masses* will tend to attract high shear stresses, and will need to fail first, for joints sets to be mobilized.

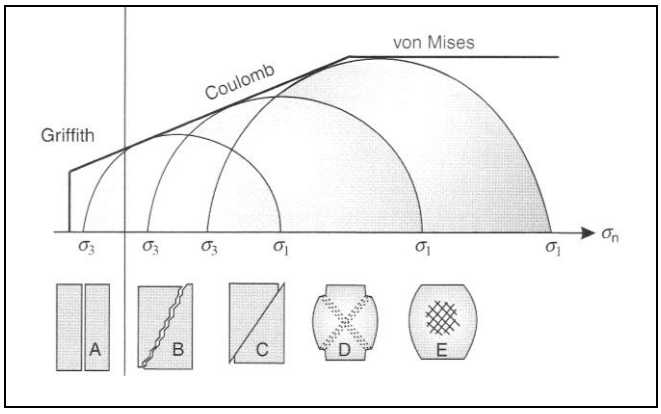

Figure 9 Representation of three classic failure criteria, and their appropriate application in terms of increasing depth or stress level, including temperature effects. After Gudmund sson, 2011. A single curvature alternative is seen in Figure 6.

3 SHEAR STRENGTH OF ROCK JOINTS

3.1 *The origin of a non-linear strength criterion*

The writer started work in rock mechanics at an opportune moment immediately following the 1st ISRM Congress in Lisbon. Patton, 1966 studies of rough joints were a source of inspiration for trying to find a quantitative alternative to his classic *i-value*. (However *'i'* can be used in combination with JRC).

The writer performed tests on numerous tension fractures, generated in various weak brittle model materials, therefore representing different lengths of fracture at prototype scale. Two of the shear test results are represented in an unusual way in Figure 10.

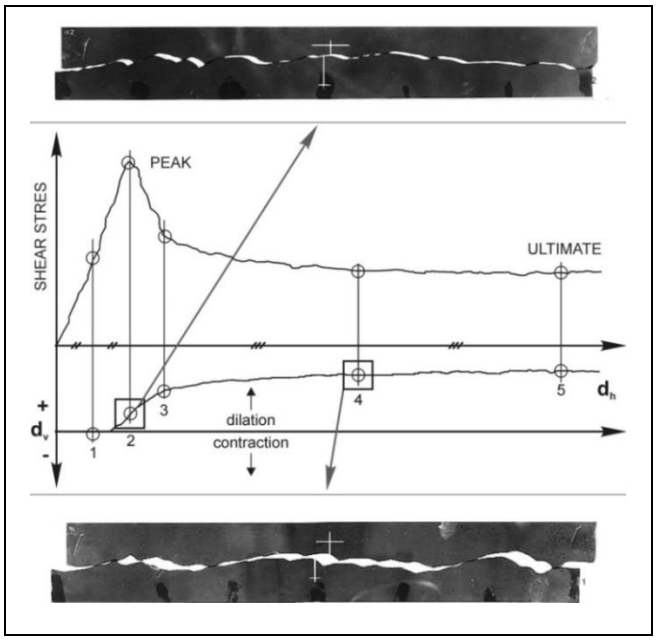

Figure 10 'Sheared roughness profiles', dating from 1968 were published in Barton, 1971, 1973. They are exactly-sheared and exactly-dilated roughness profiles of tension fractures, whose roughness was recorded by photogrammetry. Top: high σ_n/UCS ratio, bottom: low σ_n/UCS ratio. Note dilation 'void'.

These rough fractures were direct shear tested following the non-contact roughness recording. The sheared profiles are missing possible gouge from failed asperities. Nevertheless, the potential for huge permeability enhancement, and temporary 'stabilization' of a deforming rock slope was noted at the time. (Permeability with shear: Barton et al. 1985).

The peak shear strength of these rough and clearly *unweathered* tension fractures could be described by the following simple relation involving the *uniaxial compression strengths* (σ_c) of the various brittle model materials employed (Barton, 1971):

$$\tau = \sigma_n \tan [20 \log (\sigma_c/\sigma_n) + 30^o] \qquad (4)$$

This equation, derived from simple links between τ/σ_n, σ_c/σ_n and the *peak dilation angles*, proved to be 'end-member' of the Barton, 1973, and Barton and Choubey, 1977 equations for the peak shear strength of rock joints, since *unweathered tension-fractures* clearly maximise surface roughness, wall strength *and* residual friction angle. This first empirical equation was based on direct shear tests of *two hundred* artificial samples, six of which are shown in Figure 11, with their superimposed roughness profiles.

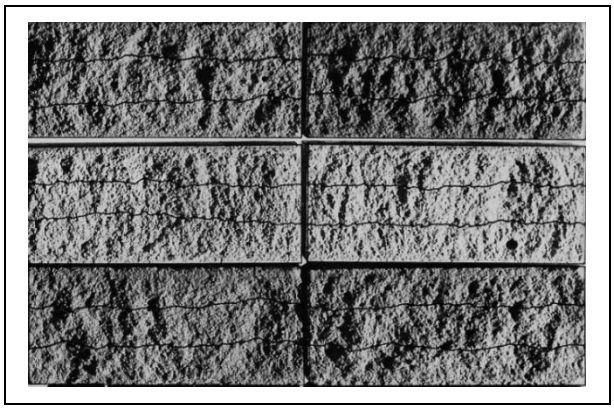

Figure 11 Six out of two hundred tension fracture samples, showing only the bottom half of the direct shear test specimens in different materials. Two roughness profiles are shown superimposed on each sample, as registered using photogrammetry. The method used is described in Wickens and Barton, 1971.

3.2 *The peak shear strength of real rock joints*

A detailed study of the shear strength and dilation characteristics of 130 *natural joint samples* was published by Barton and Choubey, 1977. (See Figs. 12, 13). Samples were sawn from larger jointed blocks extracted from rock-cuttings in the Oslo area. Seven rock types were represented. These are listed with peak shear strength results in Figure 15. Prior to direct shear testing, roughness profiling and Schmidt hammer index testing was performed, followed by self-weight tilt-testing (Figure 14) or horizontally-

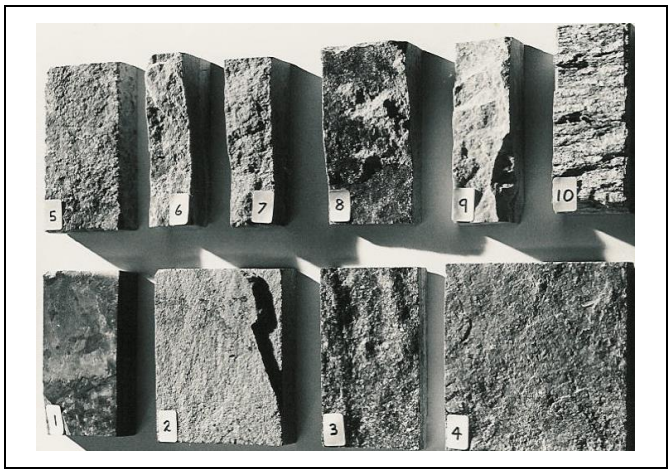

Figure 12 Ten representative joint samples with successively increasing roughness, had the roughness profiles which are reproduced in Figure 13. Sample #10 was an artificial tension fracture in soapstone. Six of these made 136 samples in total.

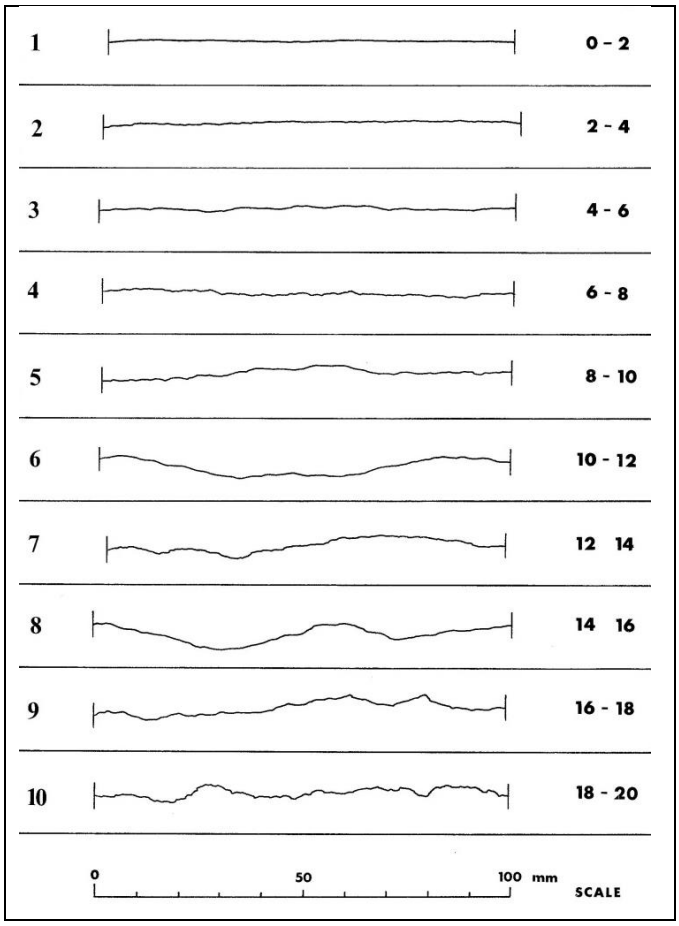

Figure 13 Ten representative roughness profiles, taken from the ten joint samples shown in Figure 12, had JRC $_{peak}$ values in the range shown on the right-hand side. Matching other joint profiles to these 'standard' profiles is obviously subjective, and tilt-testing was always advised. This advice has been repeatedly ignored by critics of JRC, who present 3D profilometer analyses, and page-wide equations, which are not helpful in rock engineering, where rapid assessment is needed.

oriented push-testing. The peak shear strength could be accurately described by the following empirical non-linear equation, which is a generalized version of equation 4. Equation 5 has existed for 37 years,

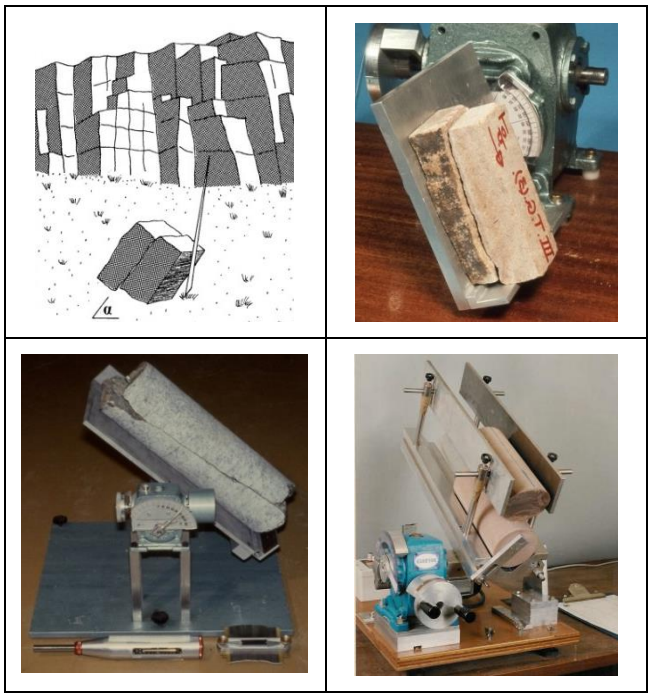

Figure 14 A variety of tilt tests are illustrated. The core sticks tested 'in line' give φ_b which usually ranges from 28-32°. Core must be unweathered, not polished, nor with ridges.

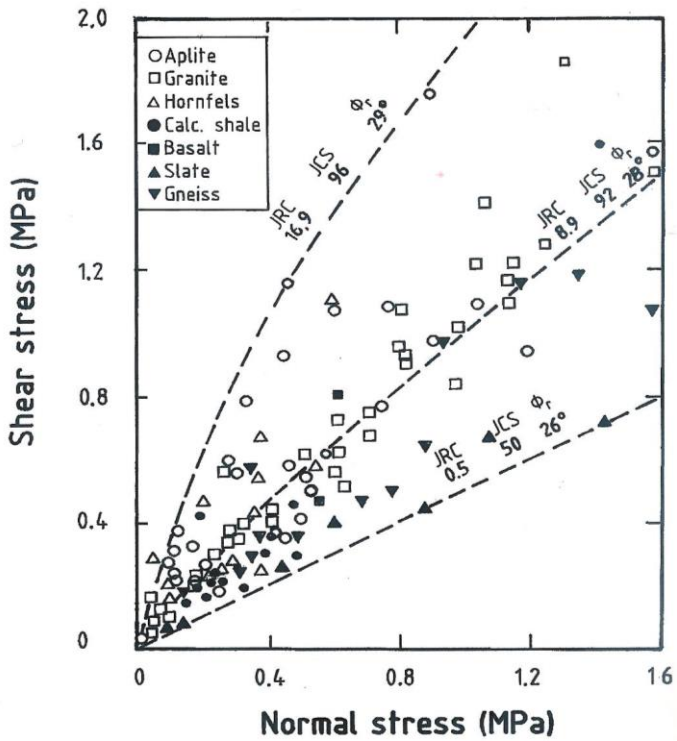

Figure 15 Fresh or slightly weathered joints in seven rock types were sawn from larger jointed blocks into 130 samples. They were direct shear tested once only (not multi-stage testing), and showed these peak strength results. Each sample was 100 mm long. Note that there is no cohesion, unless samples with vertical 'steps' are tested. Barton and Choubey, 1977.

$$\tau = \sigma_n \tan [JRC \log (JCS/\sigma_n) + \varphi_r^o] \qquad (5)$$

so the often-quoted downloadable version with an error (φ_b from Barton1973 not replaced by φ_r from 1977) was unfortunate, and led to numerous errors in refereed studies about JRC. The *joint roughness co-*

efficient (JRC), the *joint wall compression strength* (JCS) and the *residual friction angle* (φ_r) can each assume variable magnitudes, caused by variable roughness and variable weathering. In these cases JCS < σ_c and $\varphi_r < \varphi_b$. All three parameters can be measured or estimated from simple index testing, now shown in detail in Figure 16.

The *tilt-tests* can be performed on joints with JRC values from 0 to about 9, the upper limit depending on sample shape. Rougher joints need to be *push-tested*, again using self-weight (gravity) loading.

With suitably thin upper samples (to avoid toppling) the normal stress component when sliding occurs (usual α° between 50° and 80°), may be as low as 0.001 MPa. Nevertheless, the result can be extrapolated to normal stress levels 1000 to 10,000 times higher. Tens or hundreds of index tests can be performed on each important joint set recovered in jointed core, with suitable sawing parallel to the joint planes, and clamping to a heavy base in the case of Schmidt hammer tests. A smaller number of *direct shear tests* can be performed, but never by using the ISRM suggested method of *multi-stage testing*, which encourages a clockwise rotation of the resulting shear strength envelopes, due to accumulating damage. Multi-stage testing can therefore have the effect of increasing the actually non-existing 'cohesion' intercept, and reducing the friction angle, therefore artificially 'justifying' the continued use of linear Coulomb $\tau \approx$ 'c'+σ_n tan 'φ'.

When reaching the stage of rock slope design, doubt concerning the cohesion, perhaps deciding to put it as zero, results in unnecessarily conservative design. This can have serious consequences for the open-cast mining industry. Also one must never 'over-close' joints with a higher normal stress in relation to the normal stress at which shearing will occur.

In the case of rock joints with significant roughness, for instance $JRC_0 \geq$ 8-10, *over-closure* as described above has been shown to increase the steepness of the shear strength envelopes. This was shown in Barton, 1971: and subsequently documented in Barton 2007. The author knows of only four such studies, one by Bandis 1980, also by researchers in Iran.

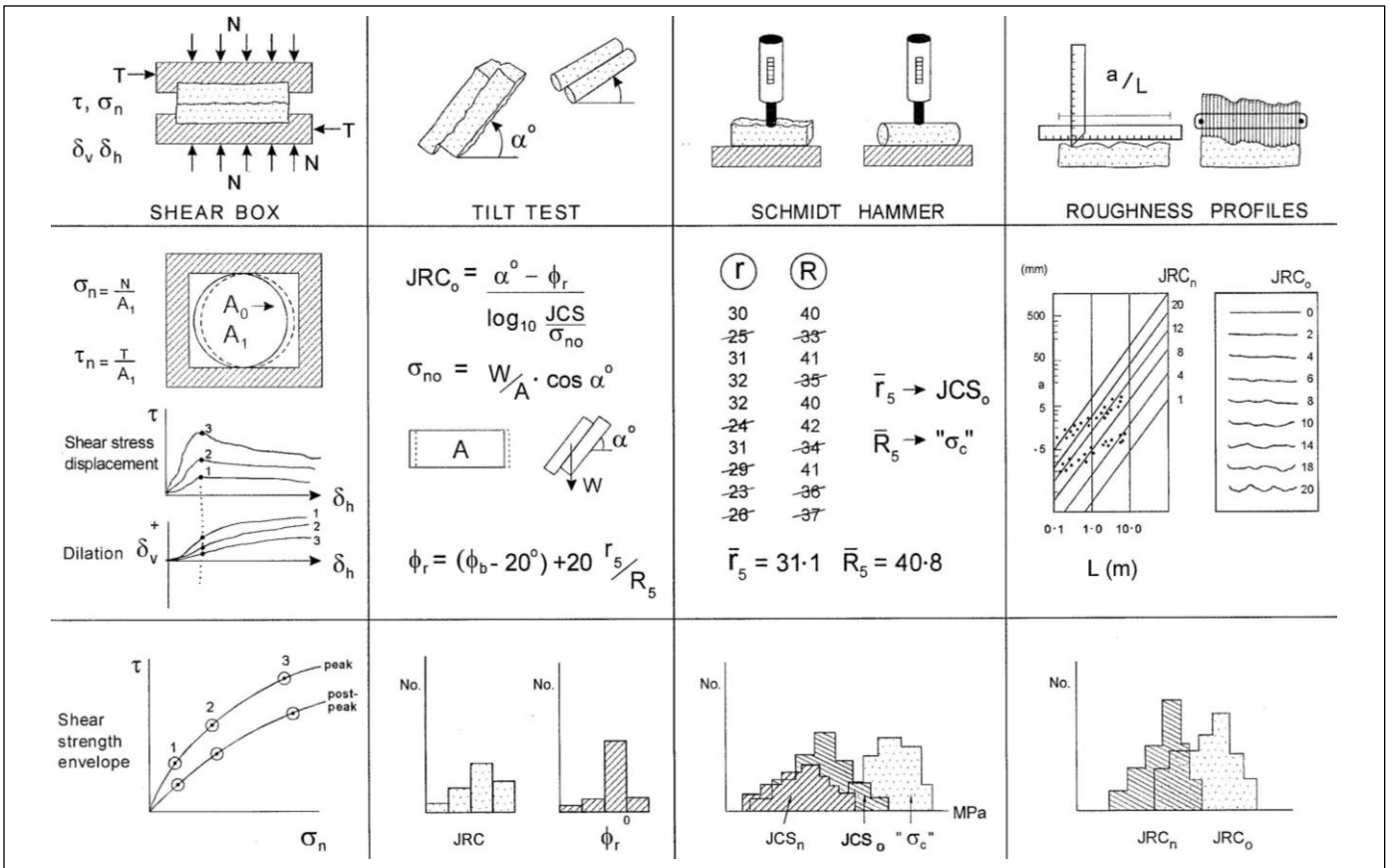

Figure 16 In the left-hand column, standard shear-box testing and typical results are shown. The objective of the index tests illustrated in the three other columns is to provide input data for JRC, JCS and φ_r, the latter estimated from measured φ_b using two core sticks (unpolished, no ridges) and using the equation with r_5 / R_5. Schmidt hammer tests give best results when the 50% of *lowest rebounds* are discarded, i.e. do not follow conventional practice. Note that when defining JRC, the R_5 (= σ_c) and φ_b tests are performed with *dry rock*, while the r_5 (=JCS) and *tilt tests* for JRC are with *matrix-saturation* (but not wet). Note two other ways of estimating JRC: profiling which is subjective, or the *a/L method* of Barton, 1981 which is favoured, especially with larger scale features to be measured. A larger figure showing the a/L method is given in Figure 21, under the heading '*Effects of joint (block) length'*. Occasionally, large-scale shear test facilities are available for testing large joint or fracture samples. Figures 23 and 24 show larger-scale JRC_n profiles, and tilt testing of 2.6 tons fractured blocks.

3.3 *Effects of large variation of normal stress*

When tested at low to moderate normal stress levels, rock joints display a huge range of shear strengths, which is 'exaggerated' if only testing lab-scale samples, as mostly the case in Figure 17a. Note some extremely high friction angles, when normal stresses are very low (<< 1 MPa) and roughness very high. There is no actual cohesion, unless steps are tested.

The high pressure results assembled in Figure 17b include data from Barton, 1976 and Byerlee, 1978. In view of the range it is surprising that tectonophysicists rely on a constant 'law' such as $\tau/\sigma_n = 0.85$ for the assumed strength of 'shallow' crustal faults.

Since the range of results is even wider at reservoir stress levels (say 50 to 150 MPa representing 2 to 6 km depth), measurements would seem to be needed. One could also try something more logical: estimation of the three strength parameters, but substitute in the high-stress version of equation 5 shown in Figure 1, using confined strength σ_1-σ_3 in place of JCS. Using a constant (10mm -based) friction angle over a wide range of stress and scale, as per Byerlee, 1978, seems to be an example of extreme optimism.

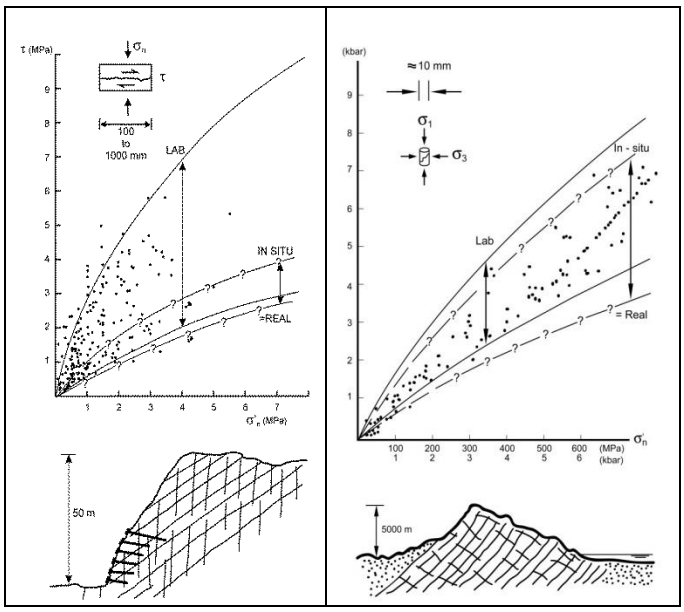

Figure 17 Left: A large assembly of DST peak shear strength results for a 'civil engineering' range of normal stresses. Note some extremely high friction angles, nevertheless no actual cohesion. Right: A large assembly of high-pressure triaxial tests, based on resolved stresses τ/σ_n. A much stronger scale effect (*in situ*?) can be assumed at low normal stress. Barton, 1990.

3.4 *Effects of joint (or block) length*

A strong impression of the importance of scale effects was experienced (Figure 18) when performing tilt tests on a joint in granite of approx. 45 cm length, and repeating the tilt tests when this large slab had been sawn into 10 cm long samples. The

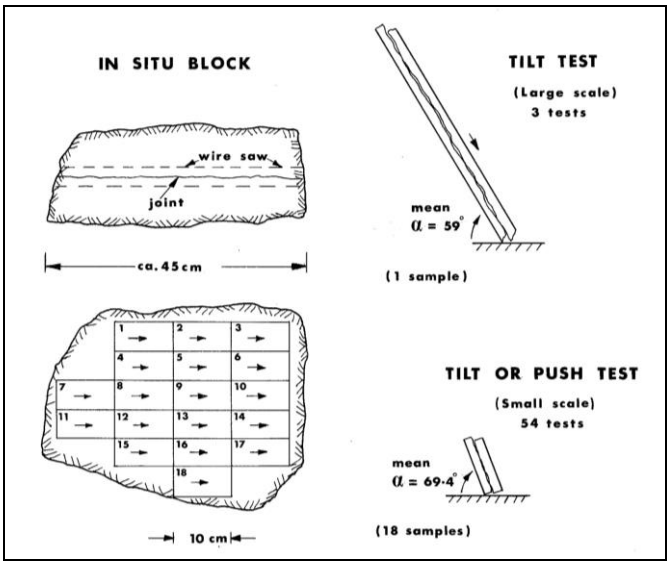

Figure 18 Tilt tests performed with different block lengths. The large-scale JRC_n was 5.5, while the mean JRC_0 was 8.7. This JRC difference will persist unchanged at high stress.

change of average tilt angle of about 10° represented a change of $JRC_n = 5.5$ (the subscript meaning large scale), to $JRC_0 = 8.7$ (the subscript meaning small scale). The eighteen 'baby' samples were sheared in the same direction as their 25 x larger 'mother' joint.

The most important scale-effect tests so far performed were by Bandis, using model materials cast as replicas of real rock joints. These could be cut into many different lengths, as illustrated in Figure 19.

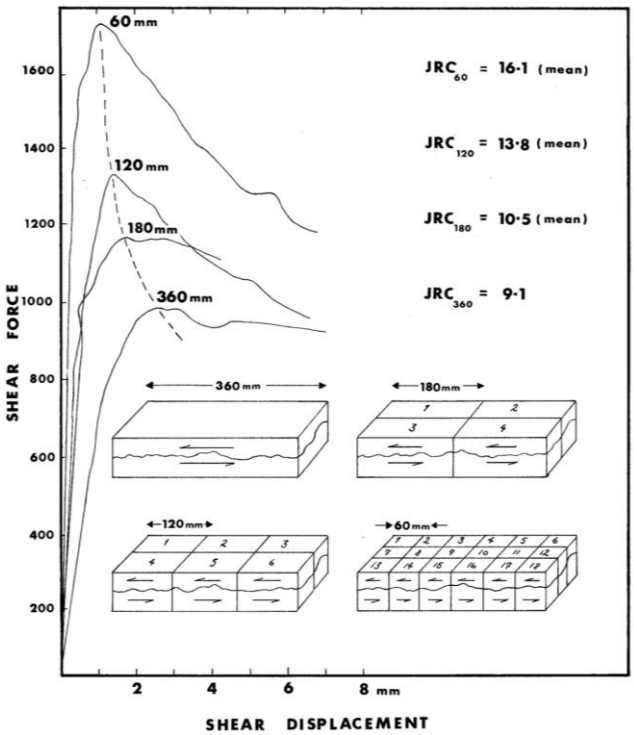

Figure 19 Direct shear-displacement tests on joint replicas by Bandis. Note strong reduction in JRC_n with block size. These important results, and many others are reproduced in Bandis et al., 1981. Note that in nature the rock joints defining small block sizes may have less roughness, or even be clay-coated.

As a result of a series of DST on rock joint replicas of many different sizes, using joints with different roughness, suggestions were made by Bandis et al., 1981 for down-scaling of JRC and JCS values for application to larger block sizes (i.e. larger cross-joint spacings). Figure 20 illustrates the method.

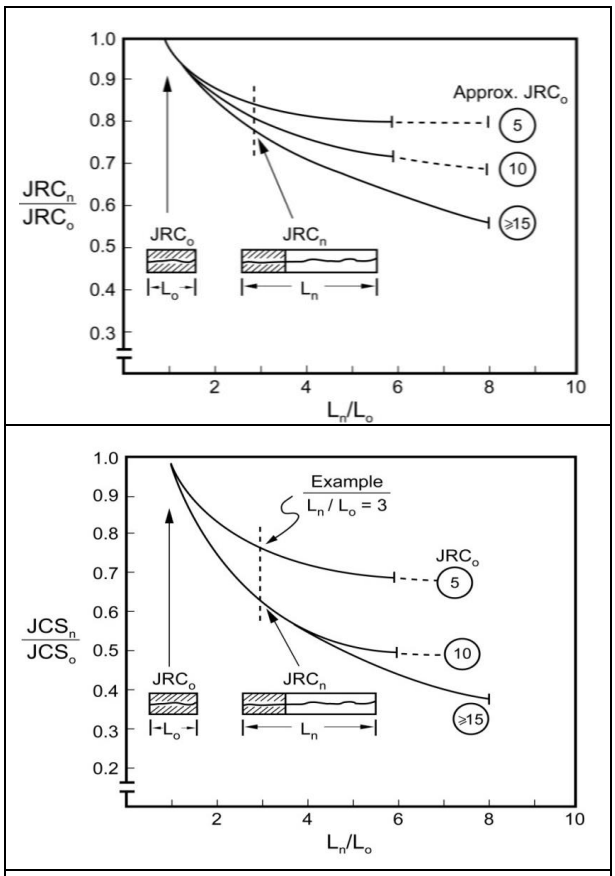

$$JRC_n \approx JRC_o \, [\, L_n/L_o \,]^{-0.02\, JRC_o}$$

$$JCS_n \approx JCS_o \, [\, L_n/L_o \,]^{-0.03\, JRC_o} \qquad (6a, 6b)$$

Figure 20 Suggested down-scaling of JRC and JCS to cross-joint spacing (block size) L_n in relation to reference lab-scale joint sample length L_o. Note that L_n is not total joint length.

An alternative way to estimate the large-scale value of JRC_n is by roughness amplitude measurement: the *a/L method*. This resembles the hydraulic engineers 'absolute roughness' which applies to the micro-roughness scale affecting hydraulic flow in joints (Barton and Quadros, 1997).

Figure 21 illustrates the 'a/L' principle of measurement for estimation of JRC_0 or JRC_n. For convenience, a chart with numerous horizontal lines is used when core- or outcrop-logging. It is possible to include a/L data for *Patton i-values*, thereby providing an 'external' addition of a larger-scale roughness *i-angle*, or its inclusion as an increased magnitude of JRC_n. These two options have not been studied sufficiently, and of course their verification is difficult.

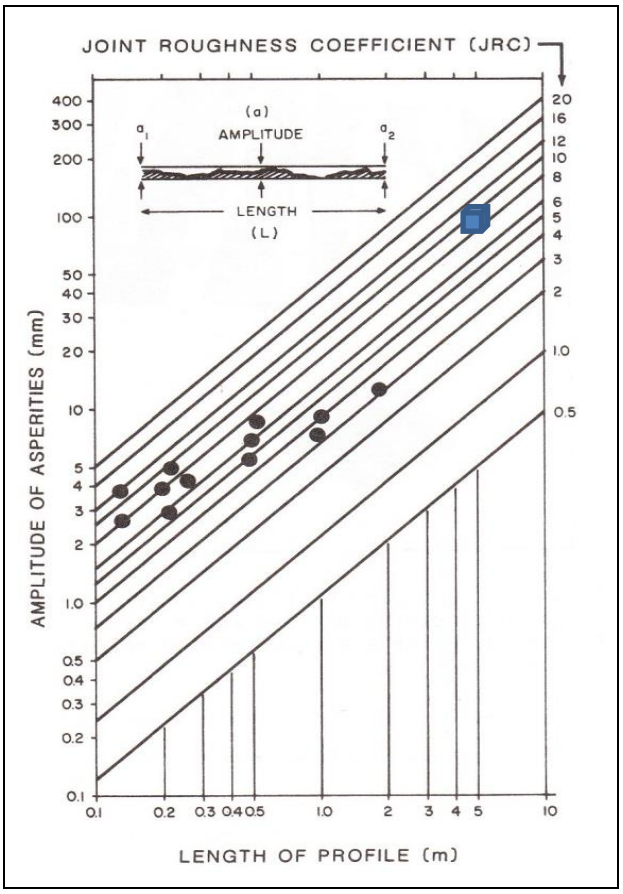

Figure 21 An alternative way to estimate JRC (and *'i'*, see cube) at different scales, from JRC_o (nominal 0.1 m lab-scale) up to 10 m, if there was a (very wide) spacing of cross-joints. A calibrated stretched steel tape can be used when beyond the limits of a 1 to 2 m high-quality folding ruler. The maximum amplitude (a) is measured in mm between contact points. When core logging, this is done very fast, as illustrated in Figure 22.

Figure 22 A suggestion for rapid a/L registration when core-logging, for easy conversion to JRC_n using the chart in Figure 21. This is by combined use of a profilometer (brush-gauge) and a ruler. Such sample orientations are of course ideal for tilt tests or push tests (both of these inexpensive and fast). A direct shear test of such samples requires sawing to DST box lengths. It is unclear why multi-stage testing is recommended by ISRM if core is available. Joint samples should not be made so scarce.

3.5 *Stress transformation problems and solutions*

Figure 23 shows problems experienced when testing large samples, due to inadequate theory. Note JRC_n for L_n = 1.1m in Figure 24 (compare to Figure 13).

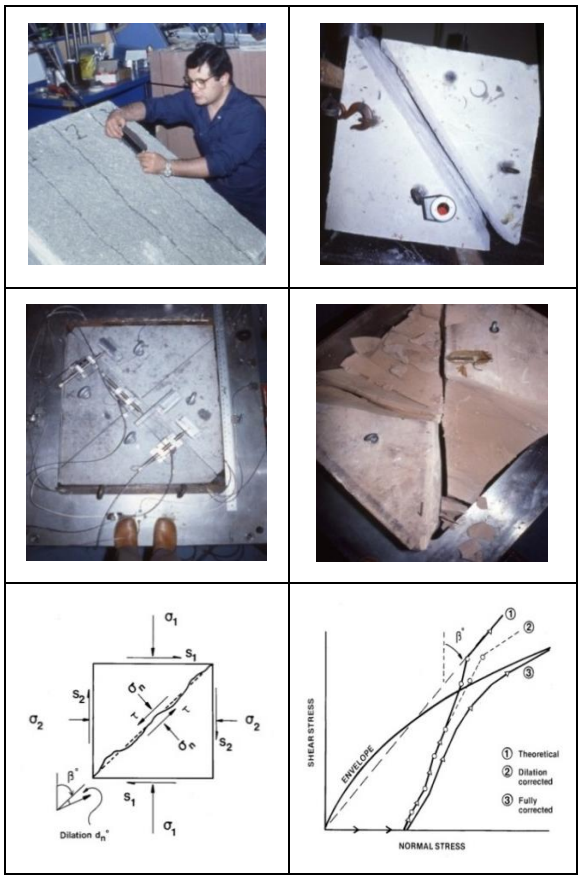

Figure 23 Large-scale (L_n = 1.1m) characterization and biaxial shear testing. Problems with shearing were experienced by Bakhtar and Barton, 1984 because of the inadequate theory for *stress transformation*, which ignores the mobilized dilation angle. Some stress-wedge-generated diagonal fractures failed to shear when expected. See Table 1 solutions (eqns. 8a, 8b, 9b).

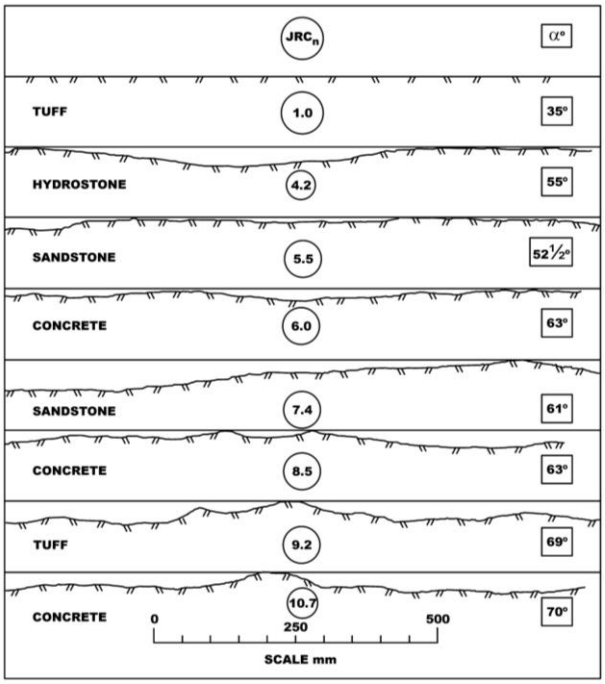

Figure 24 Roughness profiles ($L_n \approx$ 1.1m), tilt angles α° and large-scale JRC_n values, demonstrate down-scaling of JRC.

The standard stress transformation equations (7a, 7b) are based on the assumption of no actual presence of a discontinuity/joint/fracture/fault (it would disturb the assumptions), no shearing and no dilation.

Table 1 The standard and modified stress transformation equations, allowing for the mobilized dilation angles while shearing is occurring towards peak. From Bakhtar and Barton, 1984.

$\sigma_n = \frac{1}{2}(\sigma_1+\sigma_2) - \frac{1}{2}(\sigma_1-\sigma_2)\cos(2\beta)$ $\tau = \frac{1}{2}(\sigma_1-\sigma_2)\sin(2\beta)$	(7a, 7b)
$\sigma_n = \frac{1}{2}(\sigma_1+\sigma_2) - \frac{1}{2}(\sigma_1-\sigma_2)\cos[2(\beta+d_{n\,mob})]$ $\tau = \frac{1}{2}(\sigma_1-\sigma_2)\sin[2(\beta+d_{n\,mob})]$	(8a, 8b)
$d^0_{n(peak)} = \frac{1}{2}JRC_{(peak)}\log_{10}\left(\frac{JCS}{\sigma'_n}\right)$ $d^0_{n(mob)} = \frac{1}{2}JRC_{(mob)}\log_{10}\left(\frac{JCS}{\sigma'_n}\right)$	(9a, 9b)

3.6 *The JRC-mobilized concept*

This was developed by Barton, 1982, and allows one to estimate how $JRC_{mobilized}$ changes with shear displacement, reaching JRC_{peak} when the current shear displacement (δ) reaches δ_{peak}. Beyond this, roughness is degraded towards *ultimate strength*. A empirical equation in Figure 16 allows the (lower-and-difficult-to-reach) *residual friction* (φ_r) value to be estimated. It is a function of weathering grade r_5/R_5.

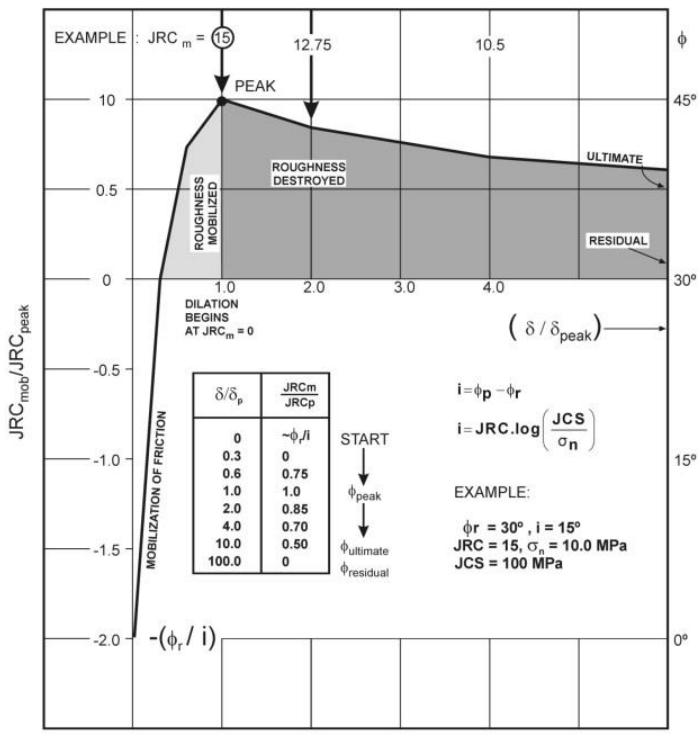

Figure 25 The $JRC_{mobilized}$ concept. This dimensionless plotting routine helps to 'consolidate' a series of shear tests performed at widely different stress levels into one narrow band representing the various shear strength versus displacement behaviours.

In Figure 26, the above dimensionless model is used together with the block-size scaling equations (Figure 20) to generate shear strength-displacement and dilation-displacement curves for three hypothetical block sizes. In the code UDEC-BB, the 'look-up' table gives a bit *smoother* curve than in Figure 25.

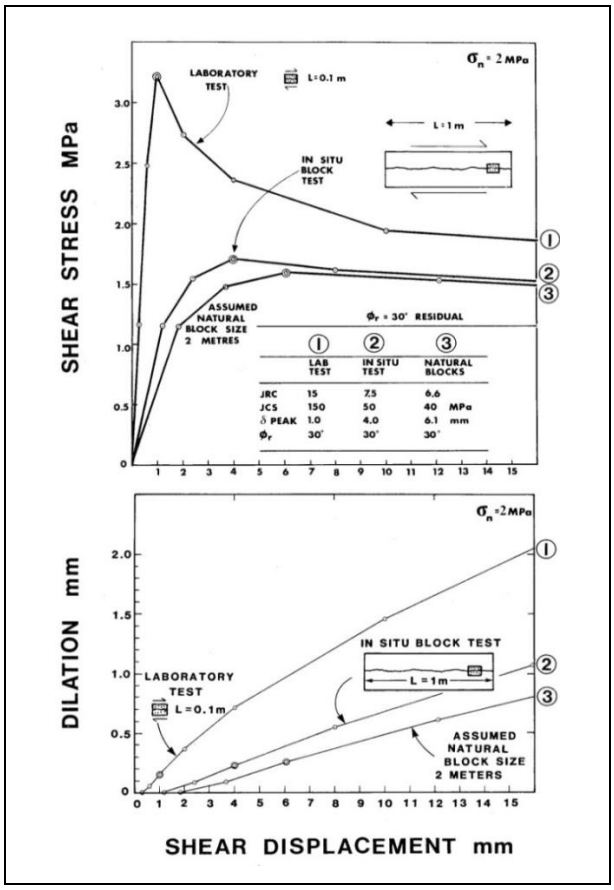

Figure 26 Examples of shear stress-displacement and dilation-displacement behaviour for lab-scale (0.1m), large-block scale (1m) and *in situ* (2m) scale. The dilation is generated using equation 9b and Figures 20 and 25. The inset shows the scaling of JRC, JCS and δ_{peak}. ($\delta_{peak} \approx 0.002L\ (JRC/L)^{0.333}$: L, δ_p in m).

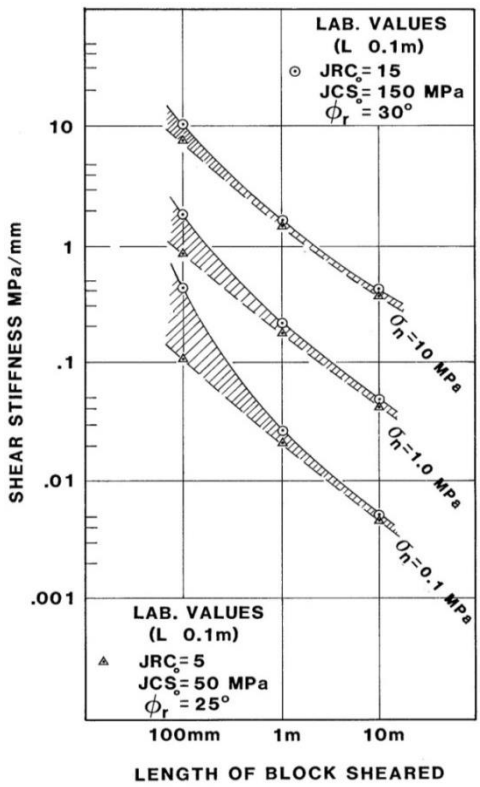

Figure 27 Shear stiffness Ks is much lower than normal stiffness Kn, as it is subject to a double scale-effect: both the peak strength and δ_{peak} are scale-dependent. In the literature Ks is often put too high. Kn/Ks may be 10/1, 50/1, even 100/1.

4 SHEAR STRENGTH OF ROCK MASSES

4.1 *Physical block models prior to UDEC*

In the days before UDEC, it was necessary (though not easy) to perform experiments with 'jointed' physical models. These like UDEC, also had the limitation of being *two-dimensional*. Nevertheless some useful lessons were learned. Figure 28 illustrates the mode of formation (double-bladed guillotine) and shows that the primary 'joint set' is continuous, and the secondary (or tertiary) sets are stepped where they cross the primary. This is 'realistic' in relation to rock masses. However the limitation is that it is difficult to make 'joint' roughness intermediate between tension fractures ($JRC_0 \approx$ 15-20) and traditionally smooth-cast model blocks ($JRC_0 \approx$ 0-1).

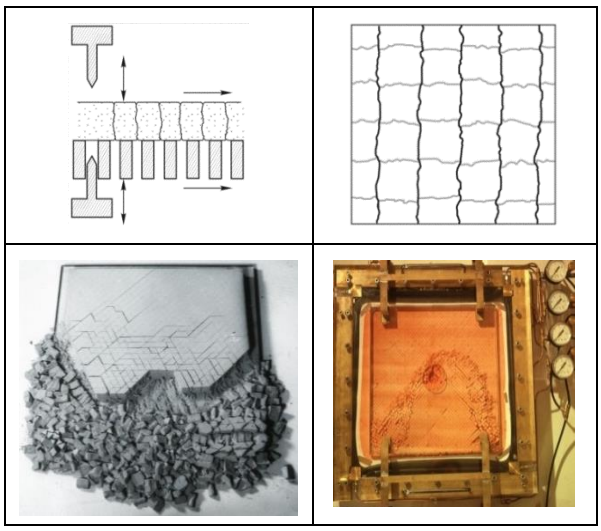

Figure 28 Prior to UDEC development, it was necessary to use physical models for studying discontinuous blocky 'rock mass' behaviour. The double-bladed guillotine (Barton, 1971) generated fracture sets with unequal properties. The biaxial test frame was used to investigate the effect of varying block size, shown in Figures 29 and 30. From Barton and Hansteen, 1979.

4.2 *Block-size dependent behaviour*

Figure 29 illustrates the importance of block size when estimating shear strength using JRC_n.

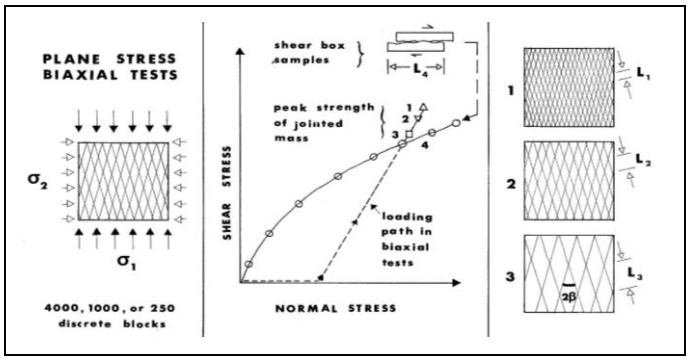

Figure 29 Biaxial shear tests with two sets of tension fractures (4,000, 1,000 or 250 blocks) showed L_n dependent strength.

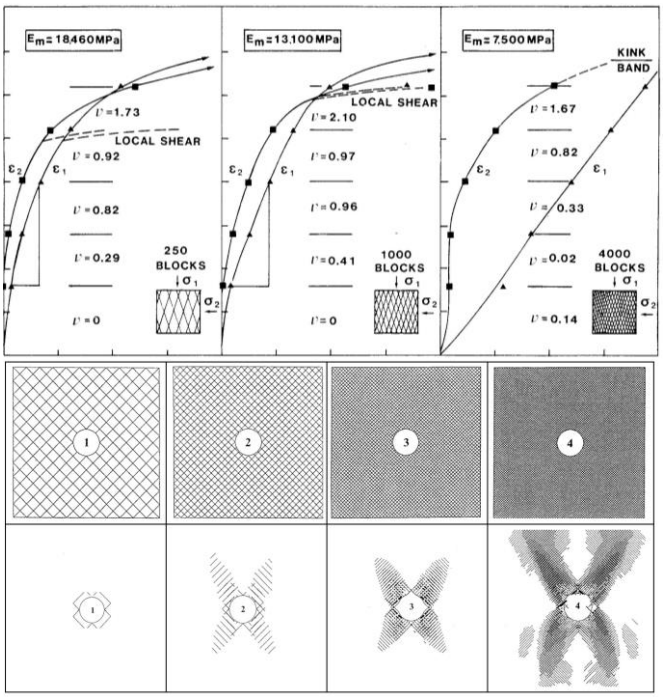

Figure 30 Top: Biaxial shearing tests with physical block-models (Barton & Hansteen, 1979) and bottom: UDEC-MC models (Shen and Barton, 1997) also with 250, 1,000, 4,000 and even 10,000 blocks. Note the dramatic effect of changing block size on shear strength - axial strain, and on block rotation potential. Note also the strong increase in lateral expansion (pseudo 'Poisson' effect). In nature small blocks may have joints with less roughness, even clay-filling, so even lower E_m.

The change to linear shear stress-axial strain behaviour (top-right), and the suddenly much deeper penetration of a tunneling-induced EDZ (bottom-right) is striking. Each occur when block size is reduced sufficiently. This may explain some of the 'unexpected events' (stoppages) experienced by TBM in fault zones, due to loosened blocks falling from the face.

The potential for heat and steam-generation within large rock-slides, causing them to travel 20 km instead of an expected 2-3 km could also be linked to block rotation. In each case when block size was reduced, there was 'preference' for a kink-band or block rotational mode, as illustrated in Figure 31.

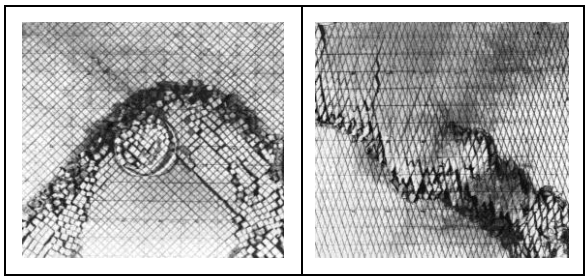

Figure 31 In each case tested with the smallest block-sizes, independent of the fracture set orientation, there was kink-band formation, then sudden *multiple-block-rotation* occurrences.

The shear resistance of rock masses is something *more complex* than complex (H-B/GSI) algebra.

4.3 *Numerical modelling and a priori shear strength*

The shear resistance of rock masses must necessarily consist of prior failure, at smallest strain, of the stiffest component, namely the intact rock bridges which may be present to resist 'simple' sliding on joint sets and along clay-filled discontinuities. The latter are mobilized at successively larger strain, which is clear when appreciating their low shear stiffness (Figure 27). Since failure is *process-and-strain dependent*, it cannot be correct as so often in the past, to add 'c' and σ_n tan 'φ', in either linear (M-C) or non-linear (H-B) form. Figure 32 is a suitable *millenium-ending* study by Hajiabdolmajid, Martin and Kaiser, 2000 'Modelling brittle failure' which demonstrates that 'standard' methods of describing and modelling failure need to be changed. Current continuum modelling, whether using linear or non-linear shear strength, falls far short of reality.

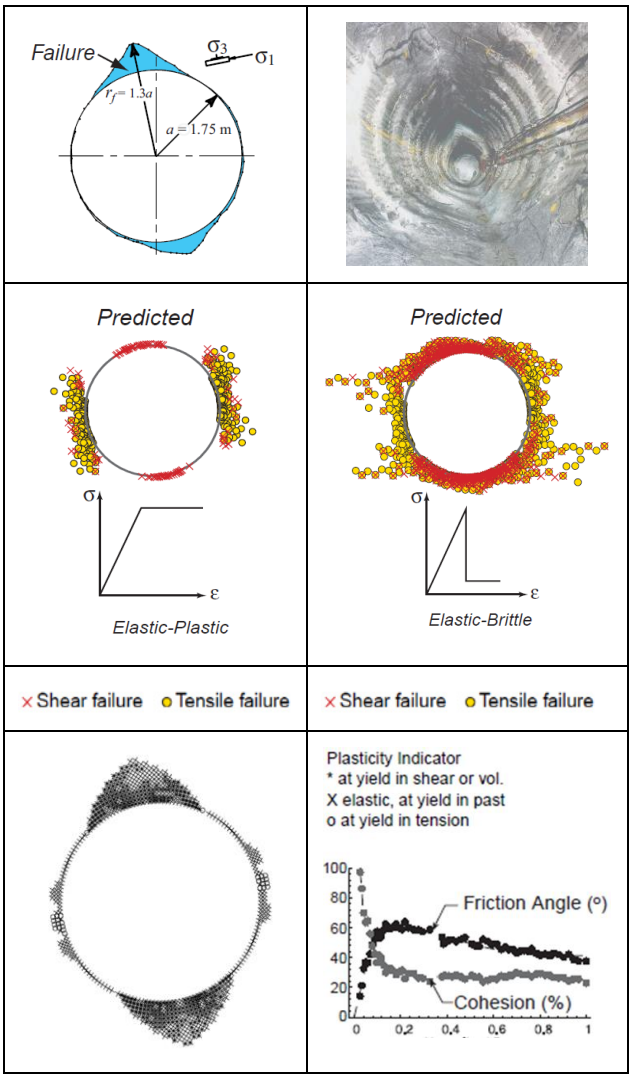

Figure 32 Attempts to use 'standard' modelling and strength criteria were unable to match an observed failure mode (top) in highly stressed granite at the URL in Canada. Even the *non-linear* Hoek-Brown, GSI-based algebra reproduced in equations 12 to 16, was unable to help this unrealistic continuum modelling, due to the conventional adding of 'c' and σ_n tan 'φ'. However, Hajiabdolmajid et al., 2000 showed an excellent match when 'c' was degraded before 'φ' was fully mobilized.

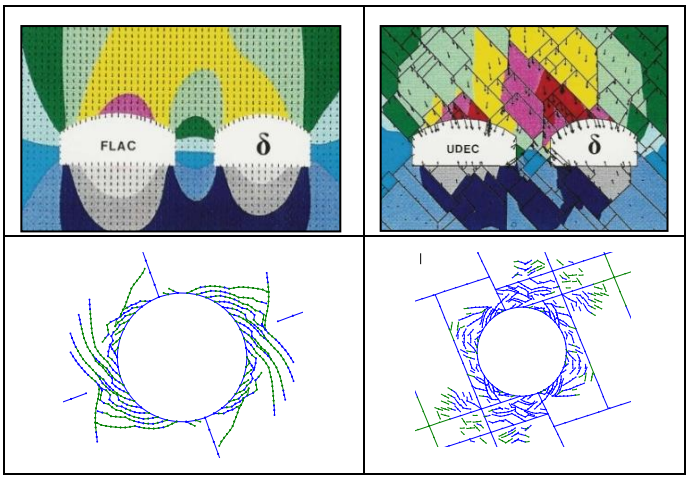

Figure 33 Top-left: Continuum models even as good as FLAC-2D fail to excite or be realistic, if shear failure is likely and strength criteria are incorrect. Top-right: Although with 2D limitations, the usual anisotropic behaviour of jointed rock masses may be captured well by UDEC and better still with UDEC-BB, since joint stiffness ratios (Kn/Ks) and shear strength should then be realistic. When a rock mass is sparsely jointed and stress-fracturing or rock bursting is expected, the use of FRACOD (Shen et al., 2013) is strongly recommended. Note the 'dispersion' of log-spiral shear fracturing when more joints are present. (Compare models: lower-left, lower-right).

4.4 *Hoek-Brown algebra or CC <u>then</u> FC*

Following the simple development of the Q to Q_c normalization ($Qc = Q \times \sigma_c/100$) to obtain better fit to seismic velocity and deformation modulus, it was also discovered (Barton, 2002) that Q_c seemed to be composed of 'c' x tan 'φ'. There is no misprint here – the multiplication is correct. This discovery was presented as Q_c = CC x FC (where Q_c = RQD/Jn x Jr/Ja x Jw/SRF x σ_c/100. CC and FC are as follows:

$$CC = (RQD/Jn) \times \sigma_c/(100.SRF) \qquad (10)$$

(the component of a rock mass requiring shotcrete for tunnel support, if the value of CC is too low)

$$FC = (Jr/Ja) \times Jw \qquad (11)$$

(the component of a rock mass requiring bolting for tunnel reinforcement, if the value of FC is too low)

CC and FC will be quantified by some examples in the next column of this paper. But first, by way of contrast to their potential simplicity and transparency, the remarkable complex-algebra Hoek-Brown/GSI formulæ for non-linear 'c' and 'φ' will be shown for reference. Table 2 also lists the GSI and D (damage) based formulæ for m_b, s and a. (σ_{3n} also needing evaluation, is based on two other parameters). There can be no set of equations in regular use in rock engineering that come close to matching all this surprising algebra. It is too easy to demonstrate complete lack of 'transparency' to e.g. an additional joint set or a clay filled discontinuity.

Table 2 Hoek-Brown/GSI based algebra for 'c' and 'φ'. This is what lies behind the 'shear strength' curves. One may wonder what happens if an extra joint set or clay-filling is added.

$c' = \dfrac{\sigma_{ci}\left[(1+2a)s+(1-a)m_b\sigma'_{3n}\right]\left(s+m_b\sigma'_{3n}\right)^{a-1}}{(1+u)(2+a)\sqrt{1+\left(6am_b\left(s+m_b\sigma'_{3n}\right)^{a-1}\right)}\Big/\left((1+a)(2+a)\right)}$	(12)
$\phi' = a\sin\left[\dfrac{6am_b\left(s+m_b\sigma'_{3n}\right)^{a-1}}{2(1+a)(2+a)+6am_b\left(s+m_b\sigma'_{3n}\right)^{a-1}}\right]$	(13)
$m_b = m_i \,.\, e^{(GSI-100)/(24-14D)}$	(14)
$s = e^{(GSI-100)/(9-3D)}$	(15)
$a = ½ + 1/6\,(e^{-GSI/15} - e^{-20/3})$	(16)

It is remarkable that so many utilize the computer-generated H-B/GSI curves of the assumed 'shear strength' of rock masses. An extremely *non*-transparent sequence of 'nested' algebra lies behind this *a priori* method. It does not encourage thought, or much needed research into the actual process-and-strain dependent shear behaviour of rock masses.

The ultra-simple and *claimed* CC and FC links to Q-system case-record needs for *shotcrete and bolting* obviously will also seem *far-fetched*, until examples of CC and FC are presented, in relation to various realistic rock mass conditions. Table 3 shows some examples, and includes established links to P-wave velocities and deformation moduli (Barton, 2002).

Table 3 Realistic Q-parameterization of successively more jointed, clay-bearing and generally weaker rock masses, and simply estimated CC (resembling MPa) and $\tan^{-1}$(FC)°.

RQD	Jn	Jr	Ja	Jw	SRF	Q	σ_c	Q_c	FC°	CC	V_p	E_m
100	2	2	1	1	1	100	100	100	63	50	5.5	46
90	9	1	1	1	1	10	100	10	45	10	4.5	22
60	12	1.5	2	0.66	1	2.5	50	1.25	26	2.5	3.6	11
30	15	1	4	0.66	2.5	0.1	33	0.04	9	0.3	2.1	3.5

Note: σ_c (MPa), CC (resembling MPa), V_P (km/s), E_m (GPa).

In multiple mine stope 3D modelling reported by Barton and Pandey, 2011, an investigation was made using conventional M-C and H-B input data, which was then applied in FLAC-3D. This was followed by modelling using (an unusual but needed) *depth-dependent* deformation modulus, and *degradation* of CC immediately followed by *mobilization* of FC.

Good agreement with pre-installed MPBX data was found, suggesting that a simple way had been found to conduct more realistic modelling, even though the performance of continuum modelling is 'undesirable' if alternatives exist for distinct element (UDEC/3DEC) modelling of e.g. individual stopes.

6 CONCLUSIONS

1. The shear strength of intact rock and the shear strength of non-planar rock joints are each non-linear, so it is hard to understand users of linear Mohr-Coulomb. It is easy but not correct.

2. In the petroleum industry, there are numerous users of 'linear behaviour'. This is despite the fact that there may be 10's of MPa increase in effective stresses during the life of a petroleum reservoir. So is rock mechanics knowledge ignored?

3. Tectonophysicists often assume $\tau/\sigma_n \approx 0.85$ (or $\varphi \approx 40°$) for shallow crustal faults, even though *10mm diameter triaxial* samples are the original basis for this assumption. There is significant variation in shear strength, even when stress levels are as high as 100 to 500 MPa. Several contributing parameters give inevitable differences.

4. Even rough tension fractures with JRC_o as high as 20, and equally rough joint surfaces, do not have cohesion. Instead they have high total friction angles due to strong dilation at very low stress. Multi-stage testing tends to create 'cohesion'.

5. Experiments with physical block models and rough tension fractures, and experiments with replicas of rock joints tested at different size, show higher JRC with smaller blocks. However, blocky rock masses often have more planar joints.

6. Rock masses reach shear failure in a *process-and-strain dependent* manner. If there are areas of intact rock ('bridges'), these attract highest stress and fail at smallest strain. Sliding on the newly formed fracture surfaces (high JRC, JCS and φ_b) progresses to surrounding joint sets (usually lower JRC, JCS and φ_r) and to nearby clay-filled discontinuities.

7. Due to the above *process-and-strain dependent* shear failure, it is not correct to add 'c' and σ_n tan 'φ', whether in a linear Mohr-Coulomb (M-C) or non-linear Hoek-Brown (H-B) algebra format. Nor is it likely to be realistic to perform only continuum analyses, since the likely mechanisms of shear failure and deformation are being ignored.

6 REFERENCES

Bakhtar, K. & Barton, N. 1984. Large scale static and dynamic friction experiments. *Proc. 25th US Rock Mechanics Symp.* Northwestern Univ., Illinois.

Bandis, S., Lumsden, A. & Barton, N. 1981. Experimental studies of scale effects on the shear behaviour of rock joints. *Int. J. of Rock Mech. Min. Sci. and Geomech. Abstr*. 18, 1-21.

Barton, N. 1971. *A model study of the behaviour of steep excavated rock slopes. Ph.D. Thesis*, Univ. of London.

Barton, N. 1973. Review of a new shear strength criterion for rock joints, *Engineering Geology*, Elsevier, Amsterdam, 7, 287-332.

Barton, N., Lien, R. & Lunde, J. 1974. Engineering classification of rock masses for the design of tunnel support. . *Rock Mechanics.* 6: 4: 189-236.

Barton, N. 1976. The shear strength of rock and rock joints. I*nt. J. Rock Mech. Min. Sci. and Geomech. Abstr*., 13, 9: 255-279.

Barton, N. & Choubey, V. 1977. The shear strength of rock joints in theory and practice. *Rock Mechanics* 1/2:1-54. Springer.

Barton, N. 1981. Shear strength investigations for surface mining. 3rd Int. Conf. on Stability in Surface Mining, AIME, Vancouver, 7: 171-192.

Barton, N. & Hansteen, H. 1979. Very large span openings at shallow depth: Deformation magnitudes from jointed models and F.E. analysis," 4th Rapid Exc. & Tunnel. Conf., RETC; Atlanta Georgia, 2: 1131-1353.

Barton, N., Bandis, S. & Bakhtar, K. 1985. Strength, deformation and conductivity coupling of rock joints. *Int. J. Rock Mech. & Min. Sci. & Geomech. Abstr*. 22: 3: 121-140.

Barton, N. 1986. Deformation phenomena in jointed rock. 8th Laurits Bjerrum Memorial Lecture, Oslo. *Geotechnique,* 36: 2: 147-167.

Barton, N. 1990. Scale effects or sampling bias? Closing lecture. *Proc. of 1st International Workshop on Scale Effects in Rock Masses,* Loen, Norway. Balkema.

Barton, N. & Quadros, E.F. 1997. Joint aperture and roughness in the prediction of flow and groutability of rock masses. Proc. of NY Rocks '97. *Linking Science to Rock Engineering.* Ed. K. Kim, Int. J. Rock Mech. Min. Sci. 34: 3-4, 907-916.

Barton, N. 2006. *Rock Quality, Seismic Velocity, Attenuation and Anisotropy.* Taylor & Francis, 729p.

Barton, N. 2007. Thermal over-closure of joints and rock masses and implications for HLW repositories. Proc. of *11th ISRM Congress,* Lisbon. 1: 109-116.

Barton, N. and S.K. Pandey, 2011. Numerical modelling of two stoping methods in two Indian mines using degradation of c and mobilization of φ based on Q-parameters. *Int. J. Rock Mech. & Min. Sci.,* 48,7: 1095-1112.

Byerlee, J.D. 1978. Friction in Rocks. *Journal of Pure and Applied Geophysics,* 116, 615-626.

Gudmundsson, A. 2011. *Rock Fractures in Geological Processes.* Cambridge University Press, 578 p.

Hajiabdolmajid,V., C. D. Martin and P. K. Kaiser,. Modelling brittle failure. *Proc. 4th North American Rock Mechanics Symposium, NARMS 2000* Seattle J. Girard, M. Liebman, C. Breeds and T. Doe (Eds), 991–998. Balkema.

Mogi, K. 1966. Pressure dependence of rock strength and transition from brittle to ductile flow. *Bull. Earthq. Res. Inst., Tokyo, 44, 215-232.*

Müller, L. 1966. The progressive failure in jointed media. *Proc. of ISRM Cong*., Lisbon, 3.74, 679-686.

Patton, F. 1966. Multiple modes of shear failure in rock. Proc. 1st. Cong. of ISRM, Lisbon. 1: 509-513.

Shen, B. & Barton, N. 1997. The disturbed zone around tunnels in jointed rock masses. Technical Note, *Int. J. Rock Mech. Min*. Sci, 34: 1: 117-125.

Shen, B., O. Stephansson, and M. Rinnie, 2013. *Modelling Rock fracturing Processes – A Fracture Mechanics Approach Using FRACOD.* Springer, 173p.

Shen, J., R. Jimenez, M. Karakus and C.Xu. 2013. A simplified failure criterion for intact rocks based on rock type and uniaxial compressive strength. *Rock Mech. & Rock Eng*. April, 2013.

Singh, M., Raj, A. and B. Singh, 2011. Modified Mohr-Coulomb criterion for non-linear triaxial and polyaxial strength of intact rocks. *Int. J. Rock Mech. Mining Sci.,* 48(4), 546-555.

Swolfs, 1977. *Contract Report*. TerraTek International, Salt Lake City.

Wickens, E.H. & Barton, N. 1971. The application of photogrammetry to the stability of excavated rock slopes. *Photogrammetric Record*, 7(37): 46-54.